Edge diffraction of creeping rays

S. J. Chapman
J. R. Ockendon
V. H. Saward*

OCIAM,
Mathematical Institute,
24-29 St. Giles,
Oxford OX1 3LB
email: chapman@maths.ox.ac.uk
tel: +44 1865 270506
fax: +44 1865 270515

January 27, 2000

*Current address: Smith Group Limited, Surrey Research Park, Guildford, Surrey GU2 5YP, U.K.

Abstract

Explicit formulae are derived for waves modelled by the scalar two-dimensional Helmholtz equation for the field that is diffracted when surface creeping rays encounter an infinitely sharp edge. Both Neumann and Dirichlet boundary conditions are analysed, and the diffracted field is found to be an order of magnitude smaller in the latter case.

1 Introduction

Creeping rays are real rays that exist in the shadow region of a finite scatterer that is illuminated by waves of sufficiently short wavelength. These rays describe the lowest order field in the shadow, which, for smooth scatterers, is exponentially small compared to the incident field. They are initiated at the scatterer horizon, where the incident rays are tangential, and they propagate repeatedly around the scatterer, progressively radiating diffracted rays tangentially to the surface, thus contributing to the scattered field in all directions. The energy lost by radiating these rays explains the exponential attenuation of the creeping field as it propagates into the shadow zone.

However, corners or edges in the shadow region may enhance the scattered field produced by the creeping rays, and this can be important in radar technology. This paper aims to describe a simple case of edge diffraction of a two-dimensional creeping ray field described by the dimensionless Helmholtz equation

$$\nabla^2\psi + k^2\psi = 0, \qquad k \gg 1, \tag{1}$$

with

$$\psi \sim e^{ikx} \text{ as } x \to -\infty, \tag{2}$$

together with a radiation condition and either

$$\frac{\partial\psi}{\partial n} = 0 \text{ or } \psi = 0 \tag{3}$$

on the scatterer.

The geometry may be as shown in Figure 1, which indicates the boundary layer structure that gives rise to the creeping ray field at the horizon H, where the scatterer is assumed to be analytic. We will not consider here the field generated at the lower tangency point.

Note that the scatterer forms a caustic for the radiating creeping rays and hence, for clarity, we refer to these rays as "shed creeping rays" when we are not close to the boundary and as "the surface creeping field" when we are in the caustic region, whose transverse dimension is $k^{-2/3}$. As usual in caustic regions, the amplitude in the surface creeping field is a factor of $k^{1/6}$ larger than in the shed creeping ray region (following a particular ray) due to the focussing effect, but this factor is dwarfed by the exponential decay of the creeping field as it propagates around the boundary.

Fortunately the mechanics of the initiation of the shed and surface creeping rays at the so-called "Fock-Leontovič" region near H need not concern us here, but they can be found, for example, in [3, 4, 6, 10]. However, in order to set up our diffraction problem near E, we do need to know the details of the surface creeping field solution.

The relevant boundary layer analysis is complicated, and can be found in [1, 5, 7, 10, 11]. The key idea is to use the ansatz

$$\psi \sim e^{iks+ik^{1/3}v(s)} \sum_{j=0}^{\infty} \frac{A_j(s,n)}{k^{j/3}} \tag{4}$$

in a region in which s, the distance along the scatterer from H, is $O(1)$ as $k \to \infty$, but n, the distance normal to the scatterer, is $O(k^{-2/3})$, where the phase-function $v(s)$ is to be determined along with the amplitude coefficients A_j. The leading-order terms give that

$$\begin{aligned} \frac{\partial^2 A_0}{\partial \hat{n}^2} - 2\frac{dv}{ds}A_0 + 2\hat{n}\kappa(s)A_0 &= 0, & (5)\\ \frac{\partial^2 A_1}{\partial \hat{n}^2} - 2\frac{dv}{ds}A_1 + 2\hat{n}\kappa(s)A_1 &= -2i\frac{\partial A_0}{\partial s}, & (6)\end{aligned}$$

where κ is the curvature, which we assume is positive, as in Figure 1 from H to E, and $n = k^{-2/3}\hat{n}$. The solution for A_0 that is outgoing as $\hat{n} \to \infty$ is

$$A_0 = \alpha_m(s)\mathrm{Ai}\left(-2^{1/3}e^{2i\pi/3}\kappa^{-2/3}\left(\hat{n}\kappa - \frac{dv}{ds}\right)\right), \tag{7}$$

and we first apply the Neumann condition $\partial\psi/\partial\hat{n} = 0$ on $\hat{n} = 0$, which implies that

$$v = v_m(s) = \xi_m e^{-2i\pi/3}2^{-1/3}\int_0^s \kappa(s')^{2/3}\, ds', \tag{8}$$

and ξ_m is the mth zero of $\mathrm{Ai}'(z)$. The amplitude α_m can be found from the solvability condition for A_1, which, after some algebra, reduces to

$$\frac{d\alpha_m}{ds} = \frac{\alpha_m}{6\kappa}\frac{d\kappa}{ds}, \tag{9}$$

giving

$$\alpha_m = \alpha_{m0}\kappa(s)^{1/6}, \tag{10}$$

where α_{m0} is constant. Hence the surface creeping field solution is the superposition

$$\psi = e^{iks}\sum_{m=0}^{\infty}\alpha_{m0}\kappa(s)^{1/6}\mathrm{Ai}\left(\xi_m - 2^{1/3}e^{2i\pi/3}\kappa(s)^{1/3}\hat{n}\right)\exp\left(ik^{1/3}\xi_m e^{-2i\pi/3}2^{-1/3}\int_0^s \kappa(s')^{2/3}ds'\right), \tag{11}$$

where α_{m0} are determined by matching to the solution near H as described in [10]. Note that because $\kappa > 0$ each term in the sum is exponentially smaller than its predecessor outside the Fock-Leontovič region near H (i.e. for $s \gg k^{-1/3}$) [1]. Hence, for the purposes of this paper, we retain only the first term α_{00}.

A similar scenario applies with Dirichlet data $\psi = 0$ on $n = 0$. Equation (11) is replaced by

$$\psi = e^{iks}\sum_{m=0}^{\infty}\beta_{m0}\kappa(s)^{1/6}\mathrm{Ai}\left(-2^{1/3}e^{2i\pi/3}\kappa(s)^{1/3}\hat{n} + \eta_m\right)\exp\left(ik^{1/3}\eta_m e^{-2i\pi/3}2^{-1/3}\int_0^s \kappa(s')^{2/3}ds'\right), \tag{12}$$

[1] Indeed, as discussed in [10], if we work to exponential accuracy and take account of Stokes phenomenon, we may find that α_{m0} may exhibit sudden rapid changes across Stokes lines.

where η_m is a zero of $\mathrm{Ai}(z)$ and the β_{m0} may also be determined by matching with the Fock-Leontovich region, subject to the same proviso about Stokes phenomenon.

Either (11) or (12) will give rise to shed creeping rays that are described by superpositions of terms

$$\psi \sim \frac{e^{ik(s+t)}}{\sqrt{t}k^{1/6}\kappa(s)^{1/6}} \exp\left(ik^{1/3}\zeta_m e^{-2i\pi/3}2^{-1/3}\int_0^s \kappa(s')^{2/3}ds'\right), \tag{13}$$

where s is the position on the boundary the ray is shed, t is distance along the shed ray, and ζ_m is ξ_m or η_m respectively. Because the amplitude decays only algebraically along these shed creeping rays, they will always be exponentially dominant over the field diffracted from E, which is where s takes its maximum value. Nevertheless, this diffracted field is of interest because of its possible importance on the "underside" of the scatterer, and because of the field that it transmits back along the body to H.

Clearly the edge diffracted field will be smaller in the case of Dirichlet data than it is with Neumann data, and we begin with the latter case, which is much the easier mathematically.

2 Edge Diffraction of Creeping Rays

2.1 Neumann boundary data

If the end of the plate is given by $s = S$ then we need to rescale near the edge by writing

$$s = S + k^{-1}\bar{s}, \tag{14}$$
$$n = k^{-1}\bar{n}, \tag{15}$$

where n is still the unscaled coordinate normal to the plate (extended by a straight line tangent to it at the edge). An enlarged diagram of the tip region of the plate is shown in Figure 2. We may expand the field in the surface creeping layer in terms of these inner coordinates to obtain that the leading-order incoming field is

$$\psi \sim C_N e^{i\bar{s}}, \tag{16}$$

where

$$C_N = \alpha_{00}\kappa_S^{1/6}\mathrm{Ai}\left(\xi_0\right)\exp\left(ikS + ik^{1/3}\xi_0 2^{-1/3}e^{-2i\pi/3}\int_0^S \kappa(s')^{2/3}ds'\right). \tag{17}$$

Hence the inner problem in the vicinity of the edge is

$$\frac{\partial^2\psi}{\partial\bar{s}^2} + \frac{\partial^2\psi}{\partial\bar{n}^2} + \psi = 0, \tag{18}$$
$$\frac{\partial\psi}{\partial\bar{n}} = 0, \quad \bar{n} = 0, \quad \bar{s} < 0, \tag{19}$$
$$\psi \sim C_N e^{i\bar{s}}, \quad \text{as} \quad \bar{n}^2 + \bar{s}^2 \to \infty, \quad \text{for} \quad \bar{n} > 0. \tag{20}$$

This inner problem is just the Sommerfeld problem [9] with the incident field parallel to the plate, with solution

$$\psi = \frac{C_N e^{-\frac{i\pi}{4}+i\bar{r}}}{\sqrt{\pi}}\mathrm{Fr}\left(-\sqrt{2\bar{r}}\sin\frac{\bar{\theta}}{2}\right), \tag{21}$$

where $\mathrm{Fr}(z)$ is the Fresnel integral

$$\mathrm{Fr}(z) = e^{-iz^2} \int_z^\infty e^{iu^2}\, du$$

and $\bar{r}$ and $\bar{\theta}$ are local polar coordinates with the $\bar{\theta} = 0$ axis parallel to the scatterer. For $\bar{\theta} \gg \bar{r}^{-1/2}$, the far-field behaviour of this inner solution is given by

$$\psi \sim C_N e^{i\bar{r}\cos\bar{\theta}} + C_N \frac{e^{i\bar{r}-3i\pi/4}}{2\sqrt{2\pi\bar{r}}\sin\bar{\theta}/2}, \quad 0 < \bar{\theta} < \pi, \tag{22}$$

$$\psi \sim C_N \frac{e^{i\bar{r}-3i\pi/4}}{2\sqrt{2\pi\bar{r}}\sin\bar{\theta}/2}, \quad -\pi < \bar{\theta} < 0. \tag{23}$$

Therefore the amplitude of the diffracted field at the tip is given by

$$A = C_N \frac{e^{\frac{-3i\pi}{4}}}{2\sqrt{2\pi kr}\sin\theta/2}, \tag{24}$$

where $r = \bar{r}/k$ and $\theta = \bar{\theta}$ are unscaled polar coordinates centred on the tip. There is a boundary layer of thickness $k^{-1/2}$ near $\theta = 0$ (the shadow boundary), whose structure is discussed in §3. The amplitude directivity pattern is shown in Figure 3.

2.2 Dirichlet Boundary Data

Now the leading-order incoming field is given by

$$\psi \sim C_D \bar{n} e^{i\bar{s}}, \tag{25}$$

where

$$C_D = -k^{-1/3} 2^{1/3} e^{2i\pi/3} \beta_{00} \kappa_S^{1/2} \mathrm{Ai}'(\eta_0) \exp\left(ikS + ik^{1/3}\eta_0 2^{-1/3} e^{-2i\pi/3} \int_0^S \kappa(s')^{2/3} ds' \right). \tag{26}$$

The inner problem is

$$\frac{\partial^2\psi}{\partial\bar{s}^2} + \frac{\partial^2\psi}{\partial\bar{n}^2} + \psi = 0, \tag{27}$$

$$\psi = 0, \quad \bar{n} = 0, \quad \bar{s} < 0, \tag{28}$$

$$\psi \sim C_D \bar{n} e^{i\bar{s}}, \quad \text{as} \quad \bar{n}^2 + \bar{s}^2 \to \infty \quad \text{for} \quad \bar{n} > 0, \tag{29}$$

and the presence of the amplitude $\bar{n}$ in (29) means that we cannot apply the Sommerfeld solution directly. If we make the substitution $\Phi = \partial\psi/\partial\bar{n}$ then Φ satisfies Helmholtz equation with the far field matching condition $\Phi \sim C_D e^{i\bar{s}}$ as $\bar{s} \to -\infty$. In addition the boundary data on the plate implies that $\partial^2\psi/\partial\bar{s}^2 = 0$ on $\bar{n} = 0$, $\bar{s} < 0$, and therefore $\partial\Phi/\partial\bar{n} = 0$ on the plate. Hence Φ satisfies the problem (18)-(20), so that

$$\Phi = \frac{C_D e^{-\frac{i\pi}{4} + i\bar{r}}}{\sqrt{\pi}} \mathrm{Fr}\left(-\sqrt{2\bar{r}} \sin\frac{\bar{\theta}}{2} \right). \tag{30}$$

Hence the solution to the inner problem (27)-(29) has the form

$$\psi = \int_0^{\bar{n}} \Phi(\bar{s}, \nu) d\nu + B(\bar{s}), \tag{31}$$

where $B(\bar{s})$ is zero for $\bar{s} < 0$. By substituting the expression for the Fresnel integral into (31) the solution may be written as

$$\psi = \int_0^{\bar{n}} \int_{((\bar{s}^2+\nu^2)^{\frac{1}{2}} - \bar{s})^{\frac{1}{2}}}^{\infty} e^{i\bar{s}} e^{iu^2} du d\nu + B(\bar{s}). \tag{32}$$

This solution may then be simplified further by making the substitution $\lambda^2 = \bar{s}^2 + \nu^2$ and interchanging the order of integration. After some manipulation this yields that for $\bar{s} < 0$ the field is given by

$$\psi = \frac{C_D e^{-\frac{i\pi}{4}}}{\sqrt{\pi}} \left(\bar{n} e^{i\bar{r}} \mathrm{Fr}\left(-\sqrt{2\bar{r}} \sin\frac{\bar{\theta}}{2}\right) + \frac{i e^{i\bar{r}} \sqrt{\bar{r}}}{\sqrt{2}} \cos\frac{\bar{\theta}}{2} + \frac{i e^{i\bar{r}}}{2} \mathrm{Fr}\left(\sqrt{2\bar{r}} \cos\frac{\bar{\theta}}{2}\right) - \frac{e^{-i\bar{s}} e^{3i\pi/4} \sqrt{\pi}}{4} \right), \tag{33}$$

while for $\bar{s} > 0$ the field is given by

$$\begin{aligned} \psi &= \frac{C_D e^{-\frac{i\pi}{4}}}{\sqrt{\pi}} \left(\bar{n} e^{i\bar{r}} \mathrm{Fr}\left(-\sqrt{2\bar{r}} \sin\frac{\bar{\theta}}{2}\right) + \frac{i e^{i\bar{r}} \sqrt{\bar{r}}}{\sqrt{2}} \cos\frac{\bar{\theta}}{2} + \frac{i e^{i\bar{r}}}{2} \mathrm{Fr}\left(\sqrt{2\bar{r}} \cos\frac{\bar{\theta}}{2}\right) \right. \\ &\quad \left. - \frac{i e^{i\bar{s}} \sqrt{\bar{s}}}{\sqrt{2}} - \frac{i e^{i\bar{s}}}{2} \mathrm{Fr}\left(\sqrt{2\bar{s}}\right) \right) + B(\bar{s}). \end{aligned} \tag{34}$$

The solution for $\bar{s} > 0$ differs from the solution for $\bar{s} < 0$ only by an arbitrary function of $\bar{s}$. Since ψ is analytic in $\bar{r} > 0$, and (33) is an analytic expression for the field in $\bar{s} < 0$, we must have

$$B(\bar{s}) = \frac{C_D e^{-\frac{i\pi}{4}}}{2\sqrt{\pi}} \left(i\sqrt{2\bar{s}} e^{i\bar{s}} + i \mathrm{Fr}\left(\sqrt{2\bar{s}}\right) e^{i\bar{s}} - \frac{e^{-i\bar{s}} e^{3i\pi/4} \sqrt{\pi}}{4} \right), \tag{35}$$

for $\bar{s} > 0$. However, the solution (33) does not satisfy the radiation condition for $s > 0$, since the last term represents an incoming wave. Thus we must subtract off the solution corresponding to this incoming wave, giving finally

$$\psi = \frac{C_D e^{-\frac{i\pi}{4}}}{\sqrt{\pi}} \left(\bar{n} e^{i\bar{r}} \mathrm{Fr}\left(-\sqrt{2\bar{r}} \sin\frac{\bar{\theta}}{2}\right) + \frac{i e^{i\bar{r}} \sqrt{\bar{r}}}{\sqrt{2}} \cos\frac{\bar{\theta}}{2} \right), \qquad -\infty < s < \infty. \tag{36}$$

For $\bar{\theta} \gg \bar{r}^{-1/2}$ the far-field behaviour is given by

$$\psi \sim C_D \bar{n} e^{i\bar{s}} + \frac{C_D e^{3\frac{i\pi}{4}}}{\sqrt{\pi}} \frac{e^{i\bar{r}} \sin\bar{\theta}}{8\sqrt{2\bar{r}} \sin^3\bar{\theta}/2}, \quad 0 < \bar{\theta} < \pi \tag{37}$$

$$\psi \sim \frac{C_D e^{3\frac{i\pi}{4}}}{\sqrt{\pi}} \frac{e^{i\bar{r}} \sin\bar{\theta}}{8\sqrt{2\bar{r}} \sin^3\bar{\theta}/2}, \quad -\pi < \bar{\theta} < 0. \tag{38}$$

Note that the term of order $\bar{r}^{1/2}$ in the far-field expansion of (36) has zero coefficient. The amplitude of the diffracted field is given by

$$A = \frac{C_D e^{3\frac{i\pi}{4}}}{\sqrt{\pi}} \frac{\sin\theta}{8(2kr)^{\frac{1}{2}} \sin^3\theta/2}; \tag{39}$$

its directivity is shown in Figure 4. As in §2.1 there is a boundary layer of thickness $k^{-1/2}$ near $\theta = 0$, which we discuss in §3. Note that $C_D = O(k^{-1/3} C_N)$, so that the amplitude of the diffracted field is $O(k^{-1/3})$ smaller with Dirichlet data than with Neumann data.

3 Discussion

The directivity patterns in Figures 3, 4 indicate the expected nonuniformity at the "shadow boundaries" near the tangent to the scatterer at E. In general, in the far-field of the inner region with $s = k^m \tilde{s}$, where $-1 < m \leq 0$, scaling in the shadow boundary is $n = k^{(m-1)/2}\tilde{n}$, corresponding to θ of order $k^{-(m+1)/2}$. With Neumann boundary data the shadow boundary transition function is the usual one, namely

$$\psi \sim \frac{C_N e^{-i\pi/4} e^{iks} e^{i\tilde{n}^2/(2\tilde{s})}}{\sqrt{\pi}} \mathrm{Fr}\left(-\frac{\tilde{n}}{\sqrt{2\tilde{s}}}\right). \tag{40}$$

With Dirichlet boudary data, because the incoming field is not a simple plane wave, the transition function changes to

$$\psi \sim \frac{k^{(m-1)/2} C_D e^{-i\pi/4} e^{iks} e^{i\tilde{n}^2/(2\tilde{s})}}{\sqrt{\pi}} \left(\tilde{n}\mathrm{Fr}\left(-\frac{\tilde{n}}{\sqrt{2\tilde{s}}}\right) + \frac{i\sqrt{\tilde{s}}}{\sqrt{2}}\right). \tag{41}$$

Note that the transverse scaling of the shadow boundary is such that it lies within the surface creeping layer, so that the approximation of the incoming field as either constant or linear in $\bar{n}$ is valid, only for $(m-1)/2 < -2/3$, i.e. for $m < -1/3$. At this scale in s the shadow boundary starts to notice that the field on the "illuminated" side is not simply a plane wave. The full structure of the surface creeping field becomes relevant, but we will not discuss this further here.

We also remark that the diffracted field sends a ray back along the upper surface of the body, which will generate creeping rays propagating in an anticlockwise direction from E as described in [3, 2, 8].

Finally we remark that we expect similar diffraction patterns when the "trailing edge" at E has nonzero included angle and when the body is modelled by a mixed boundary condition $\partial\psi/\partial n + \alpha\psi = 0$.

Acknowledgement The authors would like to thank the referees for their valuable comments and to acknowledge the stimulation we received from discussions with Dr C. Sillence.

References

[1] V. M. Babič and V. S. Buldyrev. *Short-Wavelength Diffraction Theory — Asymptotic Methods*, volume 4 of *Springer Series on Wave Phenomena*. Springer-Verlag, 1991.

[2] S. J. Chapman and V. H. Saward. Generation of creeping rays by acoustic sources on boundaries. *In Preparation*, 1999.

[3] V. A. Fock. *Electromagnetic Diffraction and Propagation Problems.* Pergamon Press, 1965.

[4] J. B. Keller. Diffraction by a convex cylinder. In *URSI Michigan Electromagnetic Wave Theory Symposium*, pages 312–321, 1955.

[5] J. B. Keller and R. M. Lewis. *Asymptotic Methods for Partial Differential Equations: The Reduced Wave Equation and Maxwell's Equations*, volume 1 of *Surveys in Applied Mathematics*, pages 1–82. Plenum Press, New York, 1995.

[6] M. Leontovič and V. A. Fock. Solution of the problem of the proagation of electromagnetic waves along the Earth's surface by the method of the parabolic equation. *J. Phys.*, 10:13–24, 1946.

[7] B. R. Levy and J. B. Keller. Diffraction by a smooth object. *Comm. Pure Appl. Math.*, 12:159–209, 1959.

[8] V. H. Saward. *Some Problems in Diffraction.* PhD thesis, University of Oxford, 1997.

[9] A. Sommerfeld. Mathematische Theorie der Diffraction. *Mathematische Annalen*, 47:317–374, 1896.

[10] R. H. Tew, S. J. Chapman, J. R. King, J. R. Ockendon, B. J. Smith, and I. Zafarullah. Scalar wave diffraction by tangent rays. *Preprint*, 1999.

[11] E. Zauderer. Wave propagation around a convex cylinder. *J. Math. Mech.*, 13:171–186, 1964.

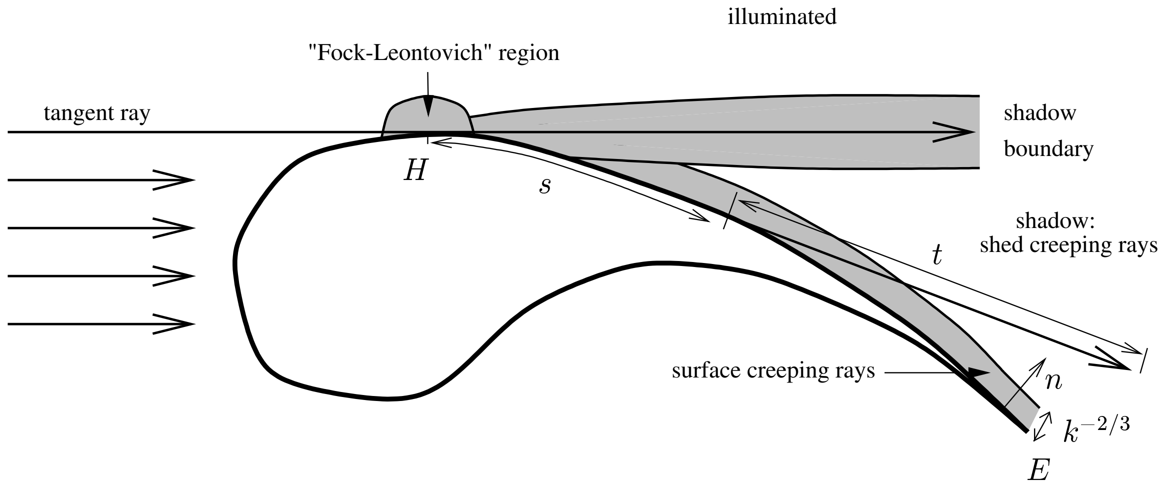
illuminated
"Fock-Leontovich" region
tangent ray
shadow
boundary
H
s
shadow:
shed creeping rays
t
surface creeping rays
n
$k^{-2/3}$
E

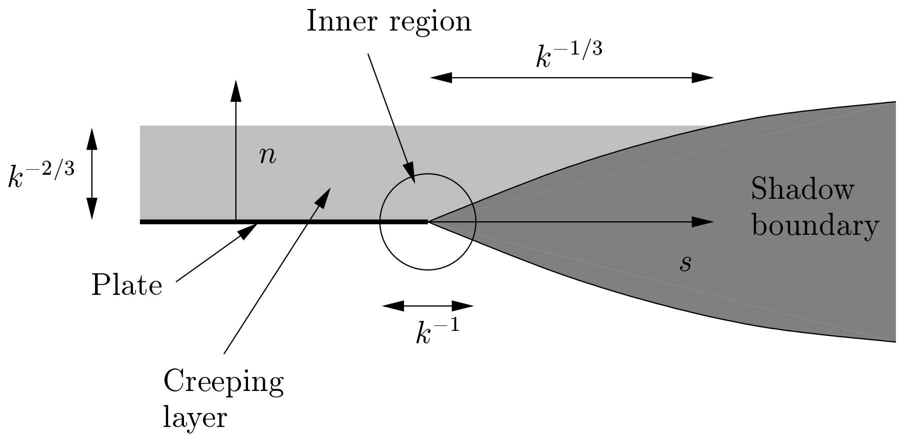
Inner region
$k^{-1/3}$
$k^{-2/3}$
n
Shadow
boundary
s
Plate
k^{-1}
Creeping
layer

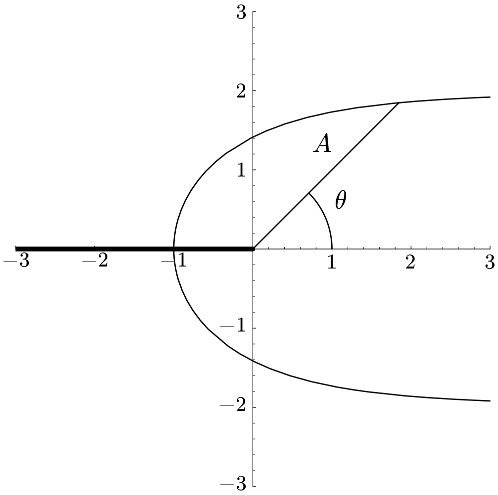

(a)

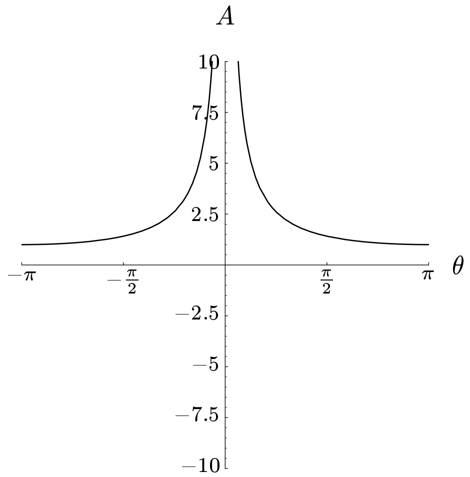

(b)

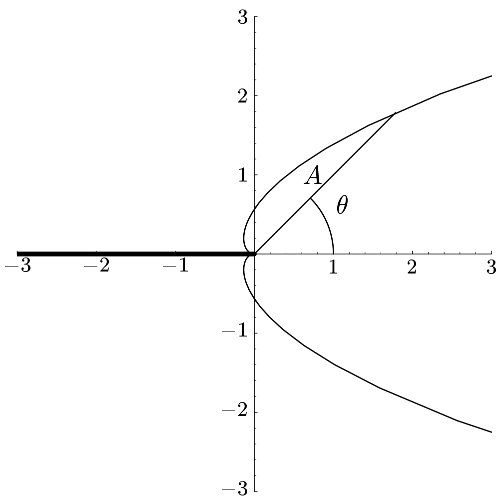

(c)

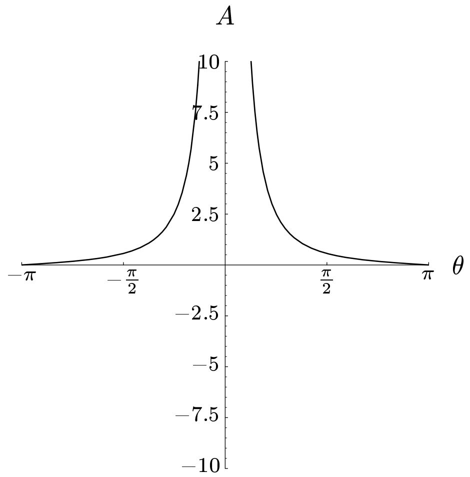

(d)

Figure captions

Figure 1: Edge diffraction of creeping rays.

Figure 2: An enlarged diagram of the tip region, showing the creeping ray layer, the inner region, and the shadow boundary region produced when the creeping rays are diffracted from the tip.

Figure 3: The directivity of the diffracted field for Neumann boundary data (a) The amplitude in any direction corresponds to the distance from the origin to the curve (b) The amplitude plotted as a function of θ.

Figure 4: The directivity of the diffracted field for Dirichlet boundary data (a) The amplitude in any direction corresponds to the distance from the origin to the curve (b) The amplitude plotted as a function of θ. The amplitude has been scaled with 0.2 as a representative value of $k^{-1/3}$, to aid in comparisons with Figure 3.